

1 **Human Foveal Cone Photoreceptor Topography and its Dependence on Eye Length**

2

3 **Authors:**

4 Wang, Yiyi¹; Bensaïd, Nicolas³; Tiruveedhula, Pavan^{1,2}; Ma, Jianqiang⁴; Ravikumar, Sowmya^{1,2};
5 Roorda, Austin^{1,2}

6

7 **Affiliations:**

8 1. School of Optometry, University of California, Berkeley, Berkeley, CA, USA

9 2. Vision Science Graduate Group, University of California, Berkeley, Berkeley, CA, USA

10 3. Carl Zeiss Meditec AG, Berlin Germany

11 4. Department of Mechanical Engineering, Ningbo University, Ningbo, Zhejiang, China

12

13 **Support:**

14 NIH/NEI grants: R01EY023591, T35EY007139, K08EY025010, P30EY003176

15

16 **Abstract:**

17 We provide the first measures of foveal cone density as a function of axial length in living eyes
18 and discuss the physical and visual implications of our findings. We used a new generation
19 Adaptive Optics Scanning Laser Ophthalmoscope to image cones at and near the fovea in 28
20 eyes of 16 subjects. Cone density and other metrics were computed in units of visual angle and
21 linear retinal units. The foveal cone mosaic in longer eyes is expanded at the fovea, but not in
22 proportion to eye length. Despite retinal stretching (decrease in cones/mm²), myopes generally
23 have a higher angular sampling density (increase in cones/deg²) in and around the fovea
24 compared to emmetropes, offering the potential for better visual acuity. Reports of deficits in
25 best-corrected foveal vision in myopes compared to emmetropes cannot be explained by
26 increased spacing between photoreceptors caused by retinal stretching during myopic
27 progression.

28

29

30

31 **Introduction**

32
 33 There has been a rapid increase in prevalence of myopia, of all magnitudes, in the period
 34 between 1971-1972 and 1999-2004 (Vitale, 2009). Across sub-populations grouped by race,
 35 ethnicity and gender, several studies report axial length of the eye to be the primary variable
 36 related to myopia (Gonzalez Blanco, Sanz Fernández, & Muñoz Sanz, 2008; X. He et al., 2015;
 37 Iyamu, Iyamu, & Obiakor, 2011). Increased axial length is associated with retinal stretching and
 38 thinning of posterior segment layers and the choroid (Fujiwara, Imamura, Margolis, Slakter, &
 39 Spaide, 2009; Harb et al., 2015) and is associated with sight-threatening, often irreversible
 40 pathologies of the retina (Morgan, Ohno-Matsui, & Saw, 2012; Verkicharla, Ohno-Matsui, &
 41 Saw, 2015). Even without any detectable pathology, the structural changes associated with eye
 42 growth ought to have functional consequences for vision.

44 ***What Do We Know About Functional Deficits in Myopia?***

45
 46 One might expect that eye growth would stretch the photoreceptor layer and would
 47 increase the spacing between cones, causing a longer eye to more coarsely sample an image
 48 relative to a shorter eye. However the situation is not that simple; the axial elongation associated
 49 with eye growth is accompanied by magnification of the retinal image (Strang, Winn, & Bradley,
 50 1998). If the enlargement of the retinal image exactly matched the stretching of the cone mosaic,
 51 then eyes of different lengths would sample the visual field similarly. In fact, in large scale
 52 studies, myopes generally attain reasonably good visual acuity with optical correction (He et al.,
 53 2004; Jong et al., 2018).

54 However, more careful inspection reveals that that myopes generally (6 out of 9 studies)
 55 have poorer angular resolution and have uniformly (3 out of 3 studies) poorer retinal resolution.
 56 **Table 1** summarizes published results from psychophysical foveal tasks.

58 **Table 1:** Summary of studies investigating foveal spatial vision and sensitivity tasks in myopia.

59

Author	Refractive error range of myopic cohort [D]	Functional tests	Results for myopes at foveal center	Suggested cause
Fiorentini & Maffei, 1976	-5.5 to -10 (n=10)	CSF	Reduced CSF	Neural insensitivity (myopic amblyopia)
Thorn, Corwin, & Comerford, 1986	-6 to -9.75 (n=13)	CSF	No difference in CSF	Global expansion
Collins & Carney, 1990	-2 to -11 (n=16)	VA, CSF	No difference in VA or CSF between low and high myopic groups with contact lens correction	NA
Strang et al., 1998	0 to -14 (n=34)	VA	Reduced VA (MAR) with increasing myopia after controlling for spectacle magnification	Retinal expansion specifically at the posterior pole; increased aberrations
Liou & Chiu, 2001	0 to >-12 (n=105 eyes)	CSF	Reduced CSF with increasing myopia	Retinal stretching and disruption, neural insensitivity (myopic)

				amblyopia)
Chui, Yap, Chan, & Thibos, 2005	-0.5 to -14 (n=60)	Grating resolution	Decreased resolution acuity in cyc/mm	Retinal expansion specifically at the posterior pole; global expansion along with ganglion cell loss
Coletta & Watson, 2006	+2 to -15 (n=17)	Interferometric grating resolution	Decreased resolution acuity in cyc/mm but not in cyc/deg	Retinal expansion specifically at the posterior pole
Atchison, Schmid, & Pritchard, 2006	+0.75 to -12.4 (n=121)	Spatial summation; interferometric grating resolution	Increased critical summation area in linear area, but not in angular area; Decreased resolution acuity in cyc/mm but not in cyc/deg	Retinal expansion specifically at the posterior pole; global expansion along with ganglion cell loss
Stoimenov, 2007	-1 to -8 (n=60)	Contrast thresholds of 20/120 letters	Lower sensitivity to contrast for letters with a fixed angular size	Morphologic changes in the retina
Rossi, Weiser, Tarrant, & Roorda, 2007	-0.5 to -3.75 (n=10)	AO-corrected VA	Reduced acuity (MAR) compared to emmetropes	Retinal expansion, neural insensitivity; neural insensitivity (myopic amblyopia)
Jaworski, Gentle, Zele, Vingrys, & McBrien, 2006	-8.5 to -11.5 (n=10)	Foveal summation thresholds; CSF	Increased critical summation area (angular) Decreased luminance sensitivity Reduced contrast sensitivity at high frequencies (cyc/deg)	Reduction in photoreceptor sensitivity; postreceptoral changes; increased aberrations
Ehsaei, Chisholm, Pacey, & Mallen, 2013	-2.00 to -9.62 (n=60)	Size threshold of high and low contrast letter targets	No difference in threshold retinal image size between myopes and emmetropes.	NA

60

61 Most notably, Atchison et al. (2006) and Coletta & Watson (2006) show clear deficits in
62 retinal resolution (cyc/mm) with increasing myopia using interferometric methods which bypass
63 the optics of the eye and Rossi et al. (2007) show significant deficits in angular resolution
64 (cyc/deg) in low myopes, even after using adaptive optics to correct for optical blur. All studies
65 the find myopic visual deficits implicate retinal stretching as a possible cause, but what is
66 actually happening structurally at the foveal center during myopic progression is not known.
67 Therefore, the aim of the current study is to more carefully investigate how the length of the eye
68 affects cone density at and near the foveal center.

69

70 *Models for How Photoreceptors Change with Eye Growth*

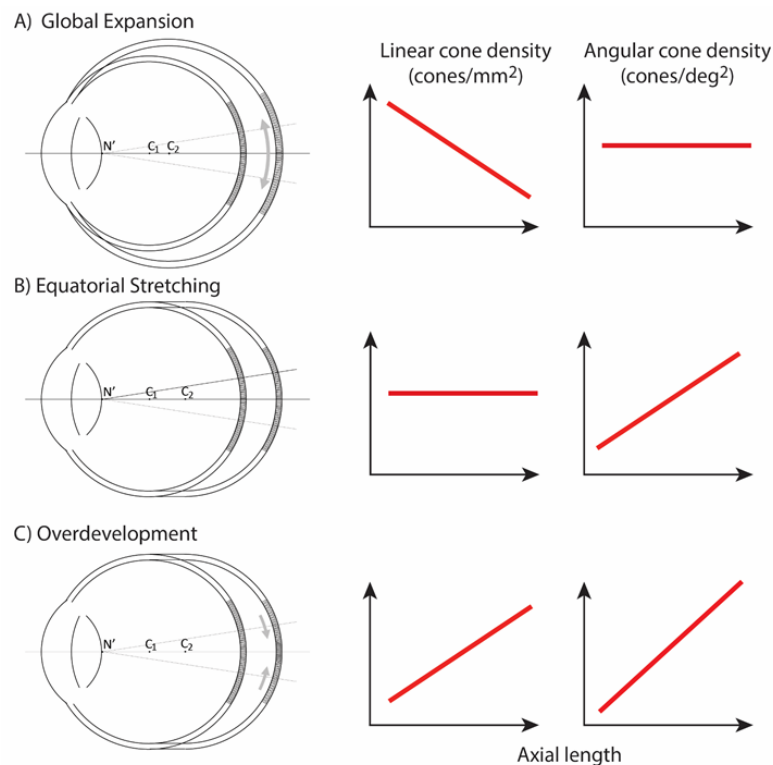
71

72 Two types of cone densities will be discussed in this study. Linear density quantifies how
73 many cones are within a fixed area, in square mm, and serves as a way to evaluate physical
74 retinal stretching caused by eye growth. Angular density quantifies how many cones are within
75 one degree visual angle, (the visual angle is measured from the secondary nodal point of the

76 eye). Angular density serves as a way to evaluate the visual implications of eye growth as it
77 governs the sampling resolution of the eye.

78 **Figure 1** illustrates three models, along the lines of Strang et al. (1998), of how
79 photoreceptor structure might be affected by myopic eye growth. In the first model, called the
80 **global expansion model**, the retina is proportionally stretched with increasing axial length -
81 cones are more spaced out in longer eyes - and linear density decreases with eye length.
82 Assuming that the secondary nodal point remains at a fixed position relative to the anterior
83 segment, the number of cones within a fixed angular area will remain constant. Therefore,
84 angular cone density will be constant with eye length. In the second model, called the **equatorial**
85 **stretching model**, the posterior retina simply moves axially further from the anterior segment of
86 the eye so that the linear density does not change with eye length. Since the retina is moving
87 further from the secondary nodal point, more cones will fall within a fixed angular area and the
88 angular cone density will increase with eye length. The final model, called the **over-**
89 **development model**, describes a structural photoreceptor change that mimics the changes that
90 occur during development (Springer & Hendrickson, 2004) whereby the photoreceptors continue
91 to migrate towards the fovea as the eye grows. In this scenario, longer eyes will show both
92 increased linear cone density and an even steeper increase in angular cone density. The model is
93 motivated by observations of increased linear cone density in the foveas of marmosets that
94 underwent lens-induced eye growth (Troilo, 1998).

95



96 **Figure 1:** 3 models of myopic eye growth: (A) Global expansion shows an eyeball that is
97 proportionally stretched. (B) The equatorial stretching model indicates a growth model where the
98 fovea stays rigid and unaffected as the eye grows. (C) The over-development model shows that
99 myopic eye growth is similar with developmental eye growth where photoreceptors continue to
100 migrate towards the fovea as the eye grows.

101

102

103 *Previous Studies of Cone Spacing with Axial Length*

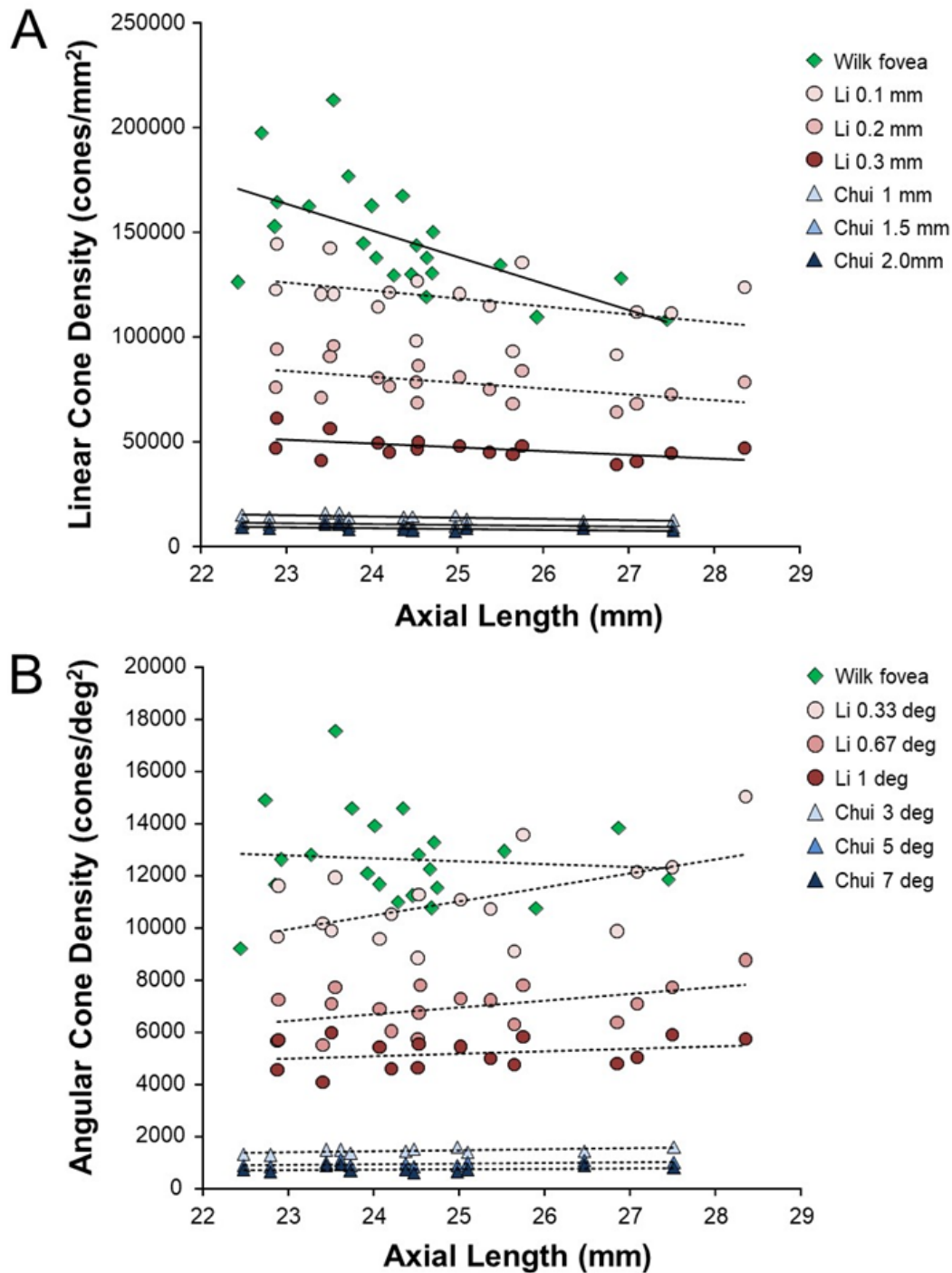
104

105 The most definitive studies of cone spacing as a function of axial length are done through
106 direct imaging of the retina – wherein sharp images of the cones are enabled through the use of
107 adaptive optics, a set of technologies that actively compensate the blur caused by aberrations of
108 the eye (Liang, Williams, & Miller, 1997). Combined with confocal scanning laser
109 ophthalmoscopy (Webb, Hughes, & Delori, 1987), adaptive optics offers the highest contrast *en*
110 *face* images of the foveal photoreceptor mosaic ever recorded in vivo (Dubra et al., 2011; Roorda
111 et al., 2002).

112 Despite continued advances in image quality, previous studies investigating cone packing
113 and eye length have not made their measurements at the foveal center, the most important region
114 for spatial vision, but the most difficult to image, owing to the small size of photoreceptors.
115 There are a number of studies on cone packing and eye length (Chui, Song, & Burns, 2008;
116 Elsner et al., 2017; Kitaguchi et al., 2007; Li, Tiruveedhula, & Roorda, 2010; Obata & Yanagi,
117 2014; Park, Chung, Greenstein, Tsang, & Chang, 2013) and here we summarize the published
118 results that are most relevant to our study. Chui et al. (2008) investigated angular and linear cone
119 density at 1 mm and 3 degrees eccentricity. They found a significant decrease ($P < 0.05$) in linear
120 cone density as a function of eye length at 1mm (which, by angular distance, is closer to the
121 fovea in a longer eye than in a shorter eye) in all directions except in the nasal retina. They found
122 that the angular cone density at 3 degrees (which, by linear distance, is closer to the fovea, in a
123 shorter eye than in a longer eye) increased with eye length, but the trends were not significant.
124 Li, et al. (2010) made similar measures, but closer to the fovea (from 0.10 mm to 0.30 mm
125 eccentricity). They found that linear cone density decreased with eye length, but the trends were
126 not significant at the smallest eccentricities (0.1 and 0.2 mm). When the data were plotted in
127 angular units and angular distance from the fovea, they found that angular cone density trended
128 toward an increase with eye length but none of the trends were significant. A more recent study
129 measured peak cone densities in the fovea as well as axial length for 22 eyes of 22 subjects (Wilk
130 et al., 2017) but they did not plot peak cone density as a function of axial length, as it was not the
131 aim of their study. We plotted the data they provided in their paper and found that the linear cone
132 density at the foveal center dropped significantly with increases in axial length, similar to what
133 was found by Li et al. (2010) and Chui et al. (2008), but the angular cone density had no
134 dependency on eye length. Summary plots from previous literature are shown in **Figures 2ab**.

135 Wilk et al. (2017)'s data were consistent with a global expansion model and Li et al.
136 (2010) and Chui et al. (2008)'s data only leaned toward a model that falls between the global
137 expansion and equatorial stretching models. If the trends found by Li et al. (2010) and Chui et al.
138 (2008) near the fovea were to extend to the foveal center, then myopes would have higher foveal
139 photoreceptor sampling resolution with a consequent potential for better performance on visual
140 tasks compared to emmetropes. As such, the simplest explanation for visual deficits in myopes –
141 increased separation between cones caused by retinal stretching – would have to be ruled out.

142 With the improvements in resolution of adaptive optics ophthalmoscopes, imaging the
143 smallest cones at the foveal center is now possible in many eyes, making it possible to complete
144 a definitive analysis of the cone density at the fovea as a function of eye length.



145
146 **Figure 2.** Summary of published data from Li et al. (2010), Chui et al. (2008) and Wilk et al.
147 (2017). In both plots, the linear fits with the solid lines indicate the data that have significant
148 trends. **(a)** Linear cone density has a decreasing trend with axial length near the fovea. **(b)**
149 Angular cone density (sampling resolution) of the eye generally increases with axial length
150 although none of the data show a significant linear relationship.

151
152

153 **Results**

154

155 The experiments were approved by the University of California, Berkeley Committee for
156 the Protection of Human Subjects. All subjects provided informed consent prior to any
157 experimental procedures. Subjects self-reported their eye health so that only healthy individuals
158 with no ocular conditions were included in the study. All eyes were dilated and cyclopleged with
159 1% Tropicamide and 2.5% Phenylephrine before imaging. We report data from 28 eyes of 16
160 subjects with a wide range of refractive error and axial length. Age, sex and ethnicity are listed
161 on **Table 2**.

162

163 ***Biometry Data***

164

165 All the biometric measures used to convert angular dimensions to linear retinal
166 dimensions are listed on **Table 2**. The strong correlation of refractive error and eye length ($P <$
167 0.0001) indicates that the subjects were predominantly as a result of axial length.

168

169 ***Imaging Data***

170

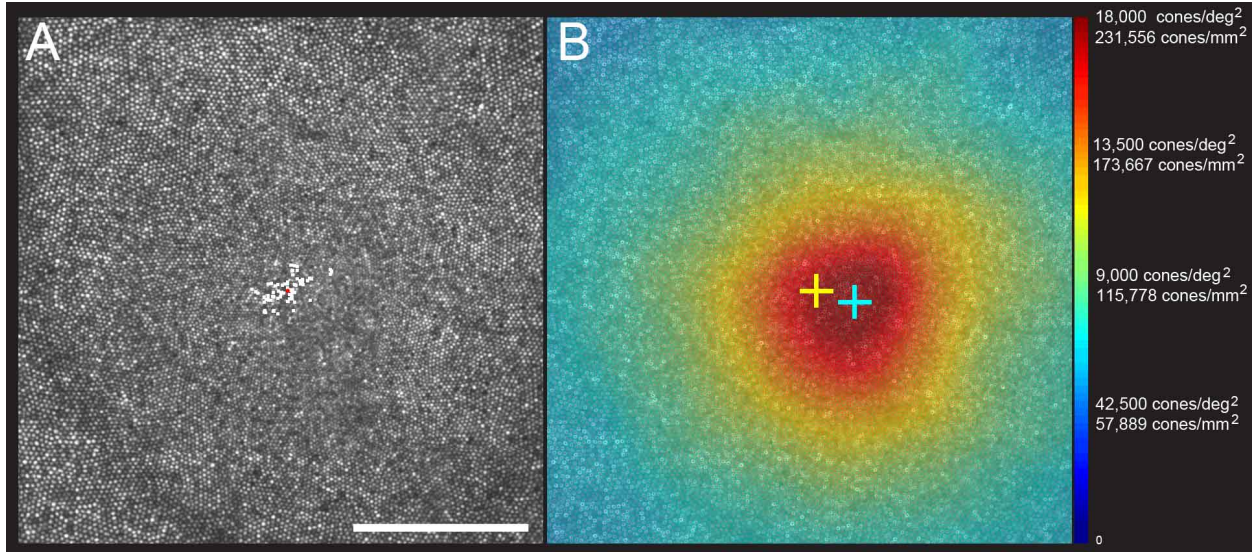
171 Images of the foveal region, the preferred retinal locus for fixation (PRL) and the fixation
172 stability were recorded with an adaptive optics scanning laser ophthalmoscope (see **Methods**
173 **and Materials**). The image of one subject (10003L) is shown in **Figure 3a**. All the cones were
174 resolved with our imaging system. The scatter plot indicates the scatter plot of fixation over the
175 course of a 10-sec video. **Figure 3b** shows the same image with all cones labeled and a color-
176 coded overlay indicating the density. 16,184 labeled cones are shown on the figure. The point of
177 maximum density is indicated by the blue cross and the average location of the PRL is indicated
178 by the yellow cross (mean of the scatter plot locations in **Figure 3a**). This eye has a peak linear
179 density of 200,482 cones/mm², and a peak angular density of 15,584 cones/deg². Cone density
180 plots in linear and angular units for all eyes are shown on **supplemental figures 1 and 2**.
181 Original images and a list of the cone locations for each can be downloaded from the Resources
182 section of the Roordalab website (roorda.vision.berkeley.edu).

183

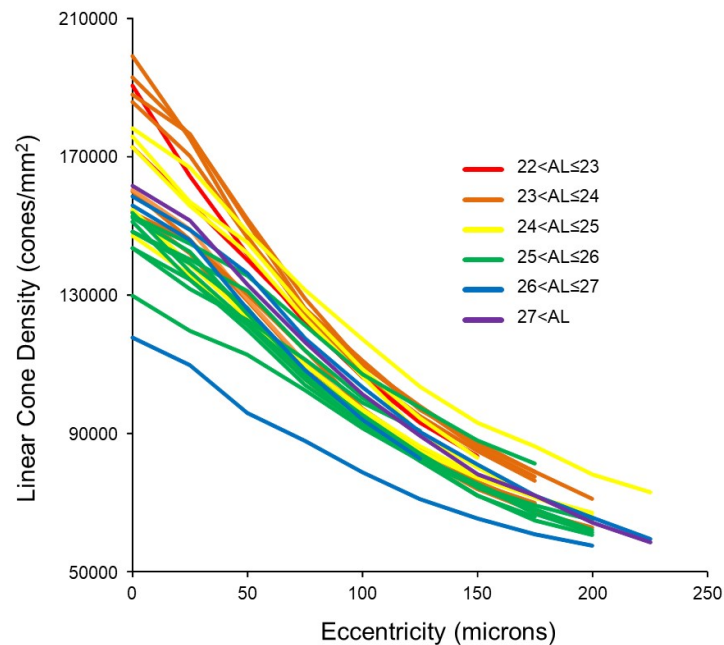
184 **Figure 4** shows the linear cone density as a function of linear eccentricity, where the
185 average linear cone density was computed in 25-micron wide annuli centered around the point of
peak density.

186 **Table 2.** Each subject's refractive error was self-reported at the time of the study. Axial Length,
 187 corneal curvature and anterior chamber depth were measure by IOL Master, and retinal
 188 magnification factor (microns/deg) was calculated from biometry data.
 189

Subject ID	Eye	Gender	Age	Ethnicity	Spherical equivalent refraction (D)	Axial length (mm)	Corneal curvature (mm)	Anterior chamber depth (mm)	Retinal magnification factor (microns/deg)	Angular cone density (cones/deg ²)	Linear Cone Density (cones/mm ²)	PRL distance from fovea (minutes)	PRL distance from fovea (microns)	PRL angular cone density (cones/deg ²)	PRL linear cone density (cones/mm ²)
20165	L	F	28	Caucasian	0.500	22.26	7.37	3.86	261.79	13247	193288	3.80	16.60	12650	184600
	R	F	28	Caucasian	0.500	22.64	7.44	3.80	267.79	12468	173857	5.48	24.45	11870	165500
20177	L	F	18	Mixed	0.000	23.04	7.80	3.24	273.59	12055	161053	7.12	32.48	11730	156800
	R	F	18	Mixed	0.000	23.23	7.91	3.20	275.85	11780	154810	4.60	21.16	11550	151800
10003	L	M	50	Caucasian	1.000	23.30	7.80	3.12	278.81	15584	200482	7.11	33.02	14070	181000
	R	M	50	Caucasian	1.000	23.50	7.81	3.14	282.00	15172	190784	4.40	20.68	14670	184400
20176	L	F	18	Asian	0.000	23.45	7.98	3.65	276.50	12513	163676	15.82	72.90	8984	117500
	R	F	18	Asian	0.000	23.58	8.01	3.62	278.52	12193	157174	3.97	18.42	11960	154200
20172	L	F	25	Caucasian	-0.750	23.56	7.71	3.90	280.13	15264	194508	2.16	10.06	15170	193300
	R	F	25	Caucasian	-0.500	23.65	7.72	3.96	281.33	14668	185324	3.43	16.08	14760	186500
20147	R	M	26	Caucasian	-0.375	24.16	7.73	2.36	298.73	15401	172581	6.17	30.70	14670	164400
	L	M	26	Caucasian	0.000	24.17	7.81	4.03	288.94	14805	177337	11.70	56.36	13570	162500
20124	L	F	26	Asian	-3.000	24.67	7.70	4.05	298.82	13843	155024	5.15	25.63	13380	149900
	R	F	26	Asian	-4.250	25.29	7.68	4.07	309.88	13659	142247	1.76	9.08	13800	143700
20174	L	F	43	Caucasian	-1.750	24.80	7.79	3.57	302.57	13476	147200	7.67	38.65	11550	126200
	R	F	43	Caucasian	-2.750	25.37	7.83	3.62	311.85	12697	130557	5.90	30.66	11640	119700
20173	R	F	22	Caucasian	-2.750	24.96	7.81	3.68	304.64	16547	178298	7.24	36.73	15910	136000
20170	R	M	26	Asian	-2.250	25.00	7.69	3.90	305.54	14393	154172	8.77	44.65	12740	136500
	L	M	26	Asian	-3.750	25.66	7.65	4.15	316.25	14759	147573	1.50	7.90	14990	149900
20138	R	F	29	Caucasian	-5.000	25.26	7.95	3.14	311.22	13568	140078	6.37	33.05	12830	132500
	L	F	29	Caucasian	-5.000	25.28	7.91	3.15	311.92	14347	147459	5.23	27.20	14300	147000
20114	R	F	24	Asian	-5.500	25.83	8.72	3.47	310.94	14393	148864	7.34	38.05	13840	143200
	L	F	24	Asian	-6.000	26.16	8.98	3.58	313.31	15584	158761	5.63	29.38	14940	152200
20160	R	F	25	Asian	-5.375	25.83	7.81	3.60	320.25	15539	151507	8.97	47.86	14810	144400
20143	R	F	23	Asian	-6.875	25.91	7.42	2.10	334.12	17051	152739	2.92	16.26	17370	155600
20158	R	F	34	Asian	-6.500	26.60	7.84	3.51	333.78	13018	116845	3.21	17.88	12740	114400
20163	R	F	25	Asian	-7.125	26.84	7.89	3.65	336.60	17922	158183	4.16	23.31	17510	154500
	L	F	25	Asian	-7.125	27.06	7.89	3.65	340.44	18793	162149	5.03	28.52	17650	152300

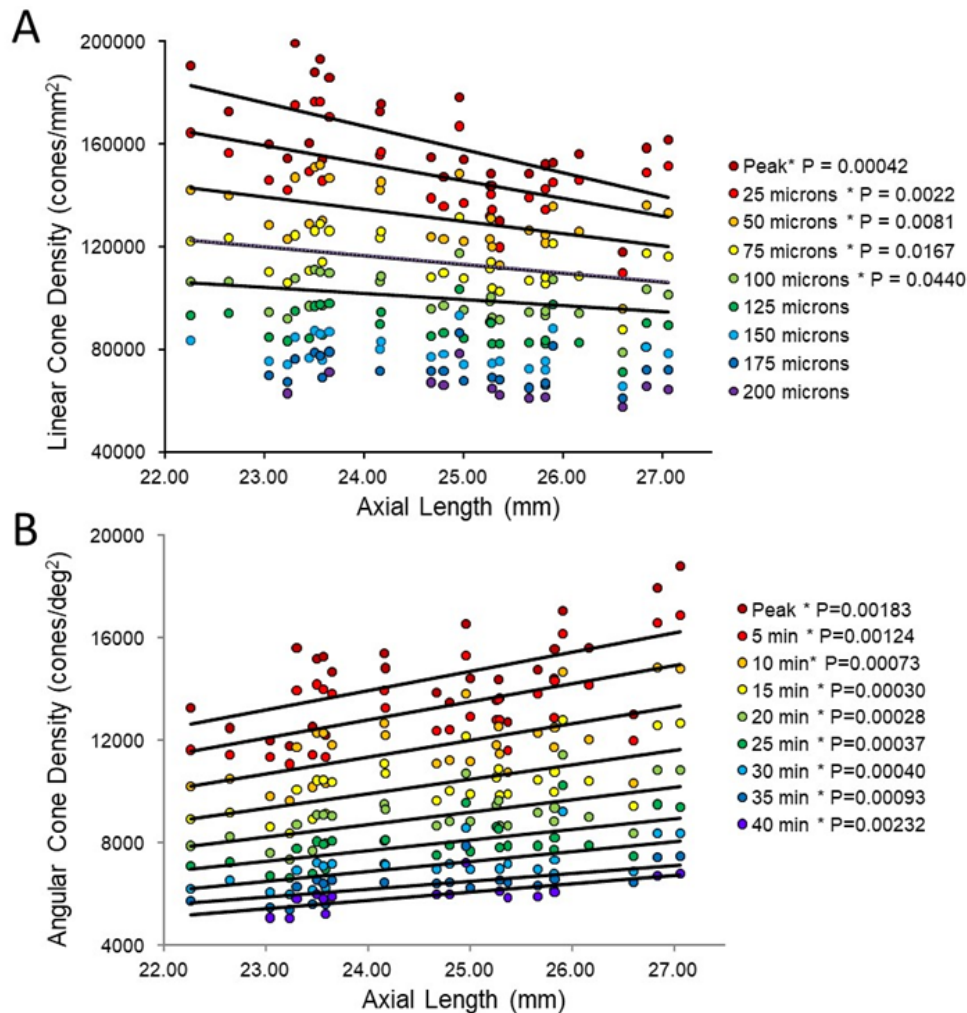


192
193 **Figure 3.** (a) AOSLO image of the fovea one subject (10003L). Only the central 1.5 degrees are
194 shown here (810 X 810 pixels), which contains 16,184 cones. The white dots are a scatter plot
195 showing the PRL, or position of the fixated stimulus over the course of a 10-second video. The
196 red dot is the centroid of the scatter plot. (b) Same image with a color overlay indicating the
197 density. Linear and angular cone densities are indicated on the right colorbar. Peak cones
198 densities in this eye are 200,482 cones/mm² and 15,584 cones/deg². The yellow and blue crosses
199 indicate the PRL and the position of peak cone density respectively. Scale bar is 0.5 degrees,
200 which in this eye corresponds to 139.4 microns.
201



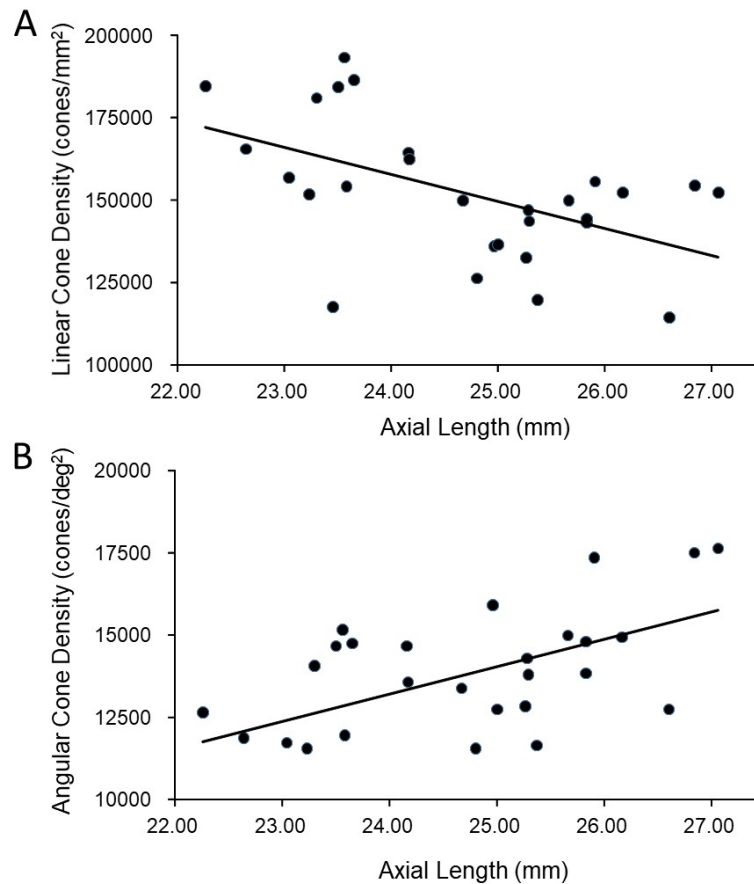
202
203 **Figure 4.** The cone density changes over different eccentricities in all the eyes. The axial length
204 ranges of the subjects are color coded, with warmer colors for shorter eyes and cooler colors for
205 longer eyes. In this plot, it is apparent that shorter eyes generally have higher peak cone
206 densities.
207

208 In order to show the trends of density with axial length **Figure 5a&b** plot linear and
209 angular cone density as a function of axial length where the colors indicate different eccentricity
210 - red to purple indicate distance from the from fovea towards more parafoveal locations. **Figure**
211 **5a** reveals that peak linear density decreases significantly with axial length and the trend persists
212 and remains significant from the fovea out to 100 microns eccentricity. Axial length accounts for
213 38% of the variance in the changes in linear cone density. **Figure 5b** shows the opposite trends
214 when plotted in angular units. Peak angular density increases significantly with axial length and
215 the trend persists and remains significant out to 40 arcminutes eccentricity. Axial length accounts
216 for 32% of the variance in the changes in angular cone density. The plots clearly indicate that
217 although stretching does occur (**Figure 5a**) it is not a simple global expansion and longer eyes
218 have higher sampling density. The trends hold at and around fovea with statistical significance.



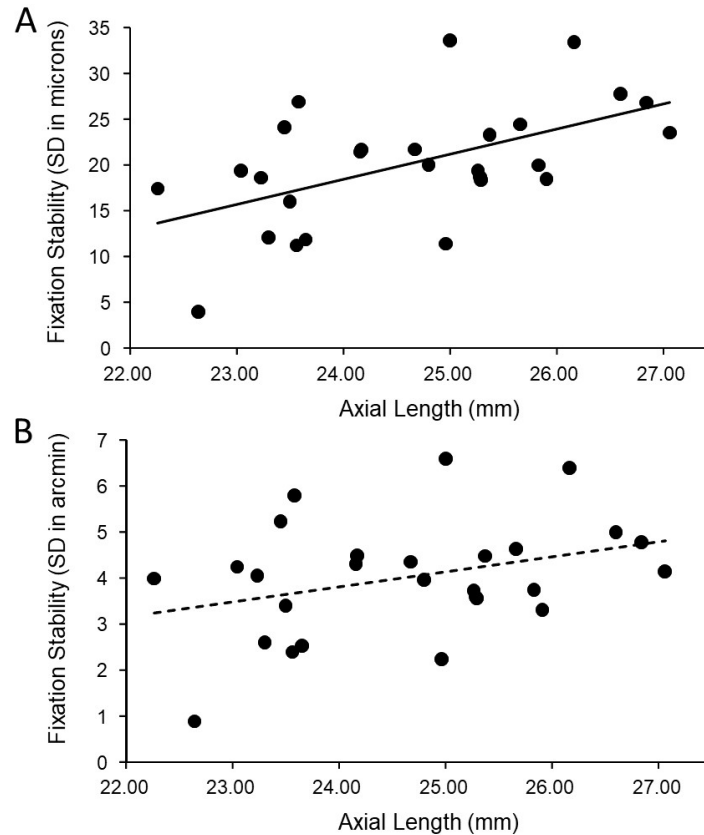
219 **Figure 5. (a)** Linear cone densities as a function of axial length. Longer eyes have lower linear
220 cone density than shorter eyes. The trend remains significant out to 100 microns eccentricity and
221 P values smaller than 0.05 are labelled with asterisks. **(b)** Angular cone densities as a function of
222 axial length. The peak angular cone density increases significantly with increasing axial length
223 and this trend remains significant out to 40 arcminutes eccentricity. The asterisks show all the
224 significant trends.
225
226

227 A more relevant measure of the impact of eye length on vision is how the angular cone
228 density changes at the PRL, which is often displaced from the location of peak cone density (Li
229 et al., 2010; Putnam et al., 2005; Wilk et al., 2017). If, for example, longer eyes had more
230 displaced PRLs then that could diminish, or even reverse, the trend of increased angular density
231 with eye length reported in **Figure 5b**. We found that the average displacement between PRL
232 and maximum cone density was 5.82 arcminutes and 28.94 microns. There was no significant
233 linear relationship found between PRL displacement in either angular or linear units vs. axial
234 length. Therefore, the PRL was not more displaced in myopes than in emmetropes from the point
235 of peak cone density. Plots of the cone density at PRL with axial length show the same trend at
236 the PRL as at the point of maximum cone density (**Figure 6 a&b**).



237 **Figure 6 ab.** The relationship between cone density and axial length shows the same pattern at
238 PRL as for the peak cone density. The slopes in both (a) and (b) are significant ($P < 0.005$) and
239 axial length accounts for 27% and 30% of the changes in linear and angular cone density,
240 respectively.
241
242

243 Finally, we explored whether fixational eye movements might have a dependency on
244 axial length. Fixation stability around the PRL had an average standard deviation of 4.0
245 arcminutes and 20.2 microns. We found a small but significant increase in the standard deviation
246 of fixational eye movement in microns with axial length (**Figure 7a**). But when we plotted it in
247 arcminutes, the trend was no longer significant (**Figure 7b**). In another words, the increase in
248 fixational eye movements in microns was just a symptom of having a longer eye.



249
250 **Figure 7. (a)** A small but significant increase in standard deviation of fixational eye movement
251 in microns was found. **(b)** when plotted in arcminutes, the trend is no longer significant.
252

253 Discussion

254
255 In this paper we measure the cone density at and near the foveal center and investigate
256 how it changes as a function of axial length. This is the first comprehensive study of cones in
257 living eyes at the foveal center, the area solely responsible for human's fine spatial vision. Our
258 results show that although some expansion does occur (linear cone density decreases with axial
259 length) the angular sampling resolution actually increases, on average, with axial length. Prior to
260 this study, the relationships between cone density and axial length were only made outside of the
261 fovea, the closest being 0.1 mm, or 0.3 degrees (Li et al., 2010). Although an eccentricity of 0.3
262 deg might seem close, it is noted that the cone density drops precipitously just outside of the
263 location of peak density (Curcio, Sloan, Kalina, & Hendrickson, 1990) as does human vision
264 (Poletti, Listorti, & Rucci, 2013)(Rossi & Roorda, 2010b). There are other factors that govern
265 peak cone density, however; eye length accounts for anywhere between 27% and 38% of the
266 variance in cone density.

267 Our finding that the slopes of cone density vs. axial length are in opposite directions
268 when plotted in linear (negative slope) and angular (positive slope) units, supports an eye growth
269 model that lies between the global expansion model and an equatorial stretching model. Previous
270 studies from our lab (Li et al., 2010) and also from (Chui, Song, & Burns, 2008) leaned in the
271 same direction. None of the cone density studies provide insight into the reasons why the
272 photoreceptor density would behave this way with eye growth, but the results do align with other

273 observations reported in the literature. Specifically, (Atchison et al., 2004) found that eyeball
274 dimensions in axial myopes are variable but are generally larger in all directions with a weak
275 tendency to be preferentially greater in the axial direction. These reported eye growth patterns lie
276 between that illustrated for the global expansion and equatorial stretching models in **figure 1**.

277 Our results differ from Wilk et al. (2017) whose data support a global expansion model
278 (i.e. there is no detectable change in angular cone density with axial length; **figure 2b**). But it is
279 important to point out that their study did not set out to address the same question and the
280 number of subjects with long axial lengths was disproportionately low.

281 Our results also differ from Troilo (1998) who studied retinal cell topography in a
282 marmoset animal myopia model. Higher cone packing densities were observed in the
283 experimentally enlarged eyes compared to normal eyes in the fovea. Their result followed the
284 overdevelopment model, which is the reason why we included it as one of the possible outcomes
285 of our study. In fact, the overdevelopment model is an extension of Springer's model of
286 development (Springer & Hendrickson, 2004), which offers a biomechanical explanation for
287 how cone packing increases at the foveal center in a developing eye. While our data do not
288 support the overdevelopment model, it does not preclude the existence of biomechanical factors
289 working in opposition to simple global expansion.

290 The fact that angular cone density (visual sampling resolution) increases with eye length
291 (myopia), at the peak density and at the PRL, means that poorer performance by myopes on
292 resolution tasks cannot be explained by a decrease in photoreceptor sampling. The deficit must
293 arise at a post-receptoral level.

294 Low-level causes for myopic visual deficits might arise from differences in the
295 connectivity between cones and ganglion cells. Atchison et al. (2006) suggested that abnormal
296 eye growth may be associated with a loss of ganglion cells. Alternately, if ganglion cells pool
297 signals from multiple cones, then they will impose the retinal sampling limit and reduce certain
298 aspects of visual performance (acuity, for example). Recent electron microscopy studies of a
299 human fovea have revealed extensive convergence and divergence connections between
300 photoreceptors and ganglion cells, albeit in an eye from an individual who was born prematurely
301 (Dacey, 2018). These discoveries challenge our current understanding of neural connectivity in
302 the foveal center and force us to consider the possibility of interindividual differences in foveal
303 cone wiring. More experiments are necessary to explore these ideas.

304 To explain why low myopes did not perform as well on an acuity task as emmetropes,
305 even after correction or bypassing of high order aberrations, Rossi et al. (2007) and Coletta &
306 Watson (2006) both raised the possibility that myopes might have become desensitized to high
307 frequency information (low level myopic amblyopia) as a result of having less exposure to a high
308 contrast visual environment. In this case, it might be possible to train myopes to take advantage
309 of their higher sampling resolution, but one myope in a follow up study by Rossi & Roorda
310 (2010a) never reached the acuity levels of emmetropes in the same study.

311 *Comparisons with Previous Studies*

312
313
314 **Peak cone densities:** Curcio et al. 1990 measured spatial density of cones and rods in
315 eight explanted whole-mounted human retinas. They found a large range of peak foveal cone
316 densities with an average of 199,000 cones/mm². When we averaged the peak cone density over
317 a circular aperture of 7.5 arcminutes which was similar to the 29 x 45 micron window that
318 Curcio et al. (1990) used to compute density, we measured peak linear cone densities ranging

319 from 123,611 to 214,895 with an average of 168,047 cones/mm². Zhang et al. (2015) reported an
320 average peak density of 168,162 cones/mm² in 40 eyes although they used a much smaller 5 x 5
321 micron sampling window to measure the peak. Wilk et al. (2017) reported an average peak
322 density of 145,900 cones/mm² in 22 eyes using a 37 x 37 micron sampling window and Li et al.
323 (2010) reported an average peak density of 150,412 cones/mm² in 4 eyes over a sampling
324 window encompassing 150 cones (approximately 37 micron diameter at the foveal center). All
325 reports of cone densities from adaptive optics studies in living eyes are lower than reports from
326 histology. Two possible reasons for this are (i) the excised tissue in Curcio et al. (1990)
327 underwent more shrinkage than estimated or (ii) the adaptive optics reports are subject to
328 selection bias, where individuals with the highest angular cone densities might have been
329 excluded because the image were less well resolved rendering the cones images too difficult to
330 label with confidence. In our study, we attempted to image 73 eyes from 46 subjects and only
331 succeeded in resolving cones across a sufficiently large region at and around the fovea in 28 of
332 them. The reason the images from 45 eyes were not analyzed was due to poor or inconsistent
333 image quality arising from a number of factors: Images from 4 eyes (3 subjects) were not
334 analyzed because their refractive errors were too high (all above -8D) and we ran into to the
335 limits of the deformable mirror's dynamic range. Images from 18 eyes (13 subjects) data were
336 not analyzed because the optics of AOSLO was not tuned well enough to resolve foveal cones
337 (those images were acquired early in the study). Images from 4 eyes (2 subjects) were not
338 analyzed because of uncorrectable image degradation caused by keratoconus and corneal
339 scarring. Images from 2 eyes (1 subject) were not analyzed because of excessive aberrations
340 caused by an orthokeratology refractive correction. The cause of poor or inconsistent image
341 quality among the remaining 17 eyes were varied, including ocular surface dryness, excessive
342 eye motion and small pupils. The average refractive error among these remaining 17 eyes was
343 about the same as the successful eyes.

344 **Anisotropic density distribution:** Like Curcio et al. (1990) and Zhang et al. (2015) we
345 found steeper drops in cone density in the superior and inferior directions compared to the nasal
346 and temporal directions. Plots of density along the two cardinal directions are shown on
347 **Supplemental Figure 3.**

348 **PRL displacements:** The distance of the PRL from the foveal center for our study (mean
349 29 microns; range 8 – 73; n = 28) roughly agrees with those of Wilk et al. (2017) (mean 63
350 microns; range 20 – 263; n = 22), Li et al. (2010) (mean 34 microns; range 3 – 92; n = 18) and
351 Putnam et al. (2005) (mean 17; range 11 – 23; n = 5). The differences in cone density between
352 the peak and the PRL were small and the trends (**Figures 5 and 6**) persisted at both locations.

353 **Spatial vision estimates:** The cone array imposes the first retinal sampling limit to human
354 spatial vision (MacLeod, Williams, & Makous, 1992; Williams, 1985) and the photoreceptor
355 row-to-row spacing (assuming an hexagonal packing structure) imposes the maximum
356 frequencies that can be relayed to later stages without aliasing. We can compute the sampling
357 limit using the following formula:

358

359
$$\text{Sampling Limit} = \frac{1}{2} \sqrt{\frac{2}{\sqrt{3}} \text{Angular Density}}$$

360

361 For the densities reported here, the potential spatial frequency resolution limits range from 58.3
362 to 73.6 cyc/deg at the peak density and 58.2 to 71.4 cyc/deg at the PRL. These correspond to

363 potential acuities ranging from 20/10.3 to 20/8.2 (based on the primary spatial frequency of the
364 three bars of a Snellen E). The cone frequency cut-offs are higher than almost all the
365 interferometric acuity limits reported by Coletta & Watson (2006), even for the emmetropic
366 subjects. The acuities are in the range of those measured from emmetropic subjects after
367 adaptive optics correction by Rossi et al. (2007). A direct comparison of foveal structure and
368 function for each of our subjects was not the scope of this study but will be the topic of future
369 investigation.

370

371 Measuring structure and function of cone photoreceptors at the foveal center – the most
372 important region of the human retina – has been one of the more challenging endeavors in vision
373 science. Fortunately, the latest generation of adaptive optics ophthalmoscopes are making it
374 easier and are facilitating new discoveries within this retinal region. The pattern of how cone
375 density changes with eye growth lands somewhere between the global expansion and equatorial
376 stretching models. The cone mosaic in longer eyes is expanded at the fovea, but not in proportion
377 to eye length. Despite retinal stretching, myopes generally have a higher angular sampling
378 density in and around the fovea compared to emmetropes. Reports of reduced best-corrected
379 central visual acuity in myopes compared to emmetropes cannot be explained by decreased
380 photoreceptor density caused by retinal stretching during myopic progression.

381

382 **Material and Methods**

383

384 ***Foveal Imaging:***

385 We used our latest generation adaptive optics scanning laser ophthalmoscope (AOSLO)
386 for foveal imaging. The system used a mirror-based, out-of-plane optical design (Dubra et al.,
387 2011), and employed a deformable mirror with a continuous membrane surface and shaped with
388 97 actuators (DM97, ALPAO, Montbonnot-Saint-Martin, France). The system scans multiple
389 wavelengths simultaneously. Each wavelength was drawn from the same broadband
390 supercontinuum source (SuperK EXTREME, NKT Photonics, Birkerød, Denmark) using a
391 custom-built fiber coupler. Wave aberrations were measured with a custom-built Shack
392 Hartmann wavefront sensor using the 940 nm channel. Images were recorded using the 680 nm
393 channel. 512 x 512 pixel videos were recorded over a 0.9 x 0.9 degree square field for an average
394 sampling resolution of 9.48 pixels per arcminute. Eye alignment and head stabilization was
395 achieved by using either a bite bar or a chin rest with temple pads. At least one 10-second video
396 was recorded at the fovea and at 8 more locations where the subjects were instructed to fixate on
397 the corners and sides of the raster, to image an entire foveal region spanning about 1.8 X 1.8
398 degrees. In order to ensure the best possible focus of the foveal cones, multiple videos were
399 taken over a range of 0.05 D defocus steps to find the sharpest foveal cones. Focus steps were
400 generated by adding a focus shape onto the deformable mirror. Online stabilization and
401 registration algorithms were used to facilitate rapid feedback on the image quality.

402

403 ***Locating the Preferred Retinal Locus of Fixation (PRL)***

404 Steady fixation was achieved at the fovea center by having the subjects fixate on a dark,
405 circular, blinking dot with a diameter of 3.16 arcminutes (30 pixels) in the center of the raster.
406 The fixation target was generated by modulating the same 680 nm scanning beam used for
407 imaging and, as such, the target's location was encoded directly into each frame of the video
408 (Poonja, Patel, Henry, & Roorda, 2005). A scatter plot of the position of the blinking dot relative

409 to the retina was generated and was used to determine the fixation stability (**figure 7**) and the
410 exact location of the PRL within the imaged cone mosaic (**Table 2, Figure 3, Supplemental**
411 **figures 1 and 2**).

412

413 *Image Processing and Analysis*

414 High quality images were generated from the recorded videos offline using custom
415 software (Matlab, The MathWorks, Inc., Natick, MA) to measure and correct for distortions
416 caused by eye movements (Stevenson & Roorda, 2005). Poor-quality frames were manually
417 excluded and registered frames were averaged into a single high signal-to-noise image. The
418 processed images were stitched together (Photoshop; Adobe Systems, Inc., Mountain View, CA)
419 to create an approximately 1.8-degree montage of the foveal cone mosaic.

420 We used custom software to identify and label individual cones in the AO retinal images.
421 The program allows the user to select a region of interest and manually add and delete cone
422 labels. A combination of both manual and automated methods (Li & Roorda, 2007) were used to
423 identify cone locations as the current version of the program does not adequately recognize cones
424 in the foveal center where they are dim and smaller (Li et al., 2010). All the cone coordinates
425 were selected and reviewed by two of the authors. In some cases cones were too dim to be seen
426 but there was only a gap in the mosaic (Bruce et al., 2015). If a space that might have been
427 occupied by a cone was dim or dark, we would assume it was a cone and mark its location. We
428 rationalize this for two reasons: First, if there is a gap in the mosaic, then it is likely that a cell is
429 occupying that space, otherwise the adjacent cells would migrate to fill it in (Scoles et al., 2014).
430 Second, in our experience and of others (Pallikaris, Williams, & Hofer, 2003), cones that appear
431 dark in one visit, can often appear bright in the next. In other cases (uncommon) the contrast was
432 low in some regions or there were interference artifacts in the images (Meadway & Sincich,
433 2018; Putnam, Hammer, Zhang, Merino, & Roorda, 2010), making the cone locations slightly
434 ambiguous. In these instances, we made manual cone selections based on the assumption that the
435 cones were all similar in size and close-packed into a nearly hexagonal array (Curcio et al.,
436 1990).

437 Continuous density maps were generated by computing cone density within a circle of 10
438 arcminutes in diameter around every pixel location across the image. We kept the area large
439 enough to generate smooth maps, but small enough to resolve local changes. Changes in density
440 with eccentricity were generated by computing the density in 5 arcminute annuli surrounding the
441 point of peak cone density. For linear density measures we used annuli with 25 micron widths.

442

443 *Retinal Magnification Factor Calculation*

444 The exact angular dimensions of the AOSLO images were computed by imaging a
445 calibrated model eye in the AOSLO system, but the conversion to linear dimensions on the
446 retinal image requires additional measurements, since the dimensions of each eye governs the
447 actual size of the image on its retina. The conversion from visual angle to retinal distance
448 requires a measurement of the axial length of the eye and an estimation of the location of the
449 secondary nodal point. We used a four-surface schematic eye model, originally proposed by Li et
450 al., 2010 to estimate the location of the secondary nodal point. The corneal first surface radius of
451 curvature, the anterior chamber depth and the axial length were for measured for each subject
452 with an IOL Master (Zeiss Meditec, Dublin, CA). The radius of the curvature of the back surface
453 of the cornea was computed as 88.31% of the front surface (Bennett, Rudnicka, & Edgar, 1994).
454 The indices of refraction of the media and the radii of curvature of the front and back lens

455 surface were taken from the Gullstrand schematic eye (Vojnikovic & Tamajo, 2013). Once
456 determined, retinal image size is related to visual angle by the equation:

457

$$458 \quad I = \tan(1^\circ)(x - AN)\theta$$

459

460 Where I is retinal image size, x is axial length, AN is the distance from the corneal apex to the
461 eye's second nodal point, and θ is the visual angle. As can be seen in **Table 2**, myopic eyes,
462 which generally have longer focal lengths, have proportionally larger retinal images.

463

464

465

466

467

468 **Competing interests:**

469

470 A.R. has a patent (USPTO#7118216) assigned to the University of Houston and the University
471 of Rochester which is currently licensed to Boston Micromachines Corp (Watertown, MA,
472 USA). Both he and the company stand to gain financially from the publication of these results.
473 No other authors have competing interests.

474

475

476

477 **References**

478

479 Atchison, D. A., Jones, C. E., Schmid, K. L., Pritchard, N., Pope, J. M., Strugnell, W. E., &
480 Riley, R. A. (2004). Eye shape in emmetropia and myopia. *Investigative Ophthalmology*
481 *and Visual Science*, *45*(10), 3380–3386. <https://doi.org/10.1167/iovs.04-0292>

482 Atchison, D. A., Schmid, K. L., & Pritchard, N. (2006). Neural and optical limits to visual
483 performance in myopia. *Vision Res*, *46*(21), 3707–3722.
484 <https://doi.org/10.1016/j.visres.2006.05.005>

485 Bennett, A. G., Rudnicka, A. R., & Edgar, D. F. (1994). Improvements on Littmann's method of
486 determining the size of retinal features by fundus photography. *Graefes Archive for*
487 *Clinical and Experimental Ophthalmology*, *32*(6), 361–367.
488 <https://doi.org/10.1007/BF00175988>

489 Bruce, K. S., Harmening, W. M., Langston, B. R., Tuten, W. S., Roorda, A., & Sincich, L. C.
490 (2015). Normal perceptual sensitivity arising from weakly reflective cone photoreceptors.
491 *Investigative Ophthalmology and Visual Science*, *56*(8), 4431–4438.
492 <https://doi.org/10.1167/iovs.15-16547>

493 Chui, T. Y. P., Song, H., & Burns, S. A. (2008). Individual Variations in Human Cone
494 Photoreceptor Packing Density: Variations with Refractive Error. *Investigative*
495 *Ophthalmology & Visual Science*, *49*(10), 4679. <https://doi.org/10.1167/iovs.08-2135>

496 Chui, T. Y., Yap, M. K., Chan, H. H., & Thibos, L. N. (2005). Retinal stretching limits
497 peripheral visual acuity in myopia. *Vision Res*, *45*(5), 593–605.
498 <https://doi.org/10.1016/j.visres.2004.09.016>

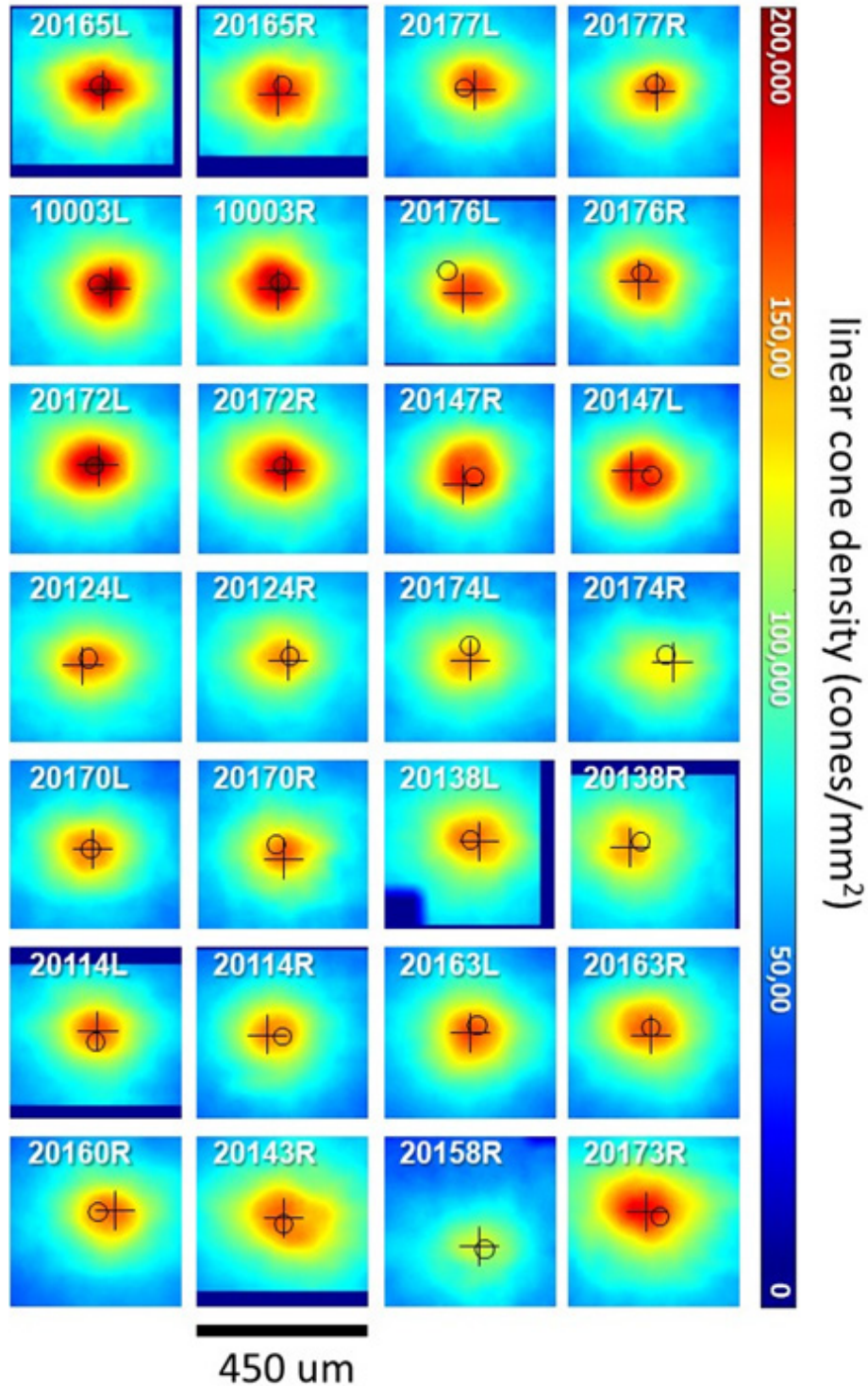
499 Coletta, N. J., & Watson, T. (2006). Effect of myopia on visual acuity measured with laser
500 interference fringes. *Vision Res*, *46*(5), 636–651. [https://doi.org/S0042-6989\(05\)00268-3](https://doi.org/S0042-6989(05)00268-3)

- 501 [pii]r10.1016/j.visres.2005.05.025
- 502 Collins, J. W., & Carney, L. G. (1990). Visual performance in high myopia. *Current Eye*
- 503 *Research*, 9(3), 217–224. <https://doi.org/10.3109/02713689009044516>
- 504 Curcio, C. A., Sloan, K. R., Kalina, R. E., & Hendrickson, A. E. (1990). Human photoreceptor
- 505 topography. *Journal of Comparative Neurology*, 292(4), 497–523.
- 506 <https://doi.org/10.1002/cne.902920402>
- 507 Dacey, D. M. (2018). Discovering visual pathway origins in the center of the human foveola
- 508 with connectomics. *Investigative Ophthalmology and Visual Science*, 59(9), ARVO
- 509 Abstract #14.
- 510 Dubra, A., Sulai, Y., Norris, J. L., Cooper, R. F., Dubis, A. M., Williams, D. R., & Carroll, J.
- 511 (2011). Noninvasive imaging of the human rod photoreceptor mosaic using a confocal
- 512 adaptive optics scanning ophthalmoscope. *Biomedical Optics Express*, 2(7), 1864.
- 513 <https://doi.org/10.1364/BOE.2.001864>
- 514 Ehsaei, A., Chisholm, C. M., Pacey, I. E., & Mallen, E. A. H. (2013). Visual performance fall-off
- 515 with eccentricity in myopes versus emmetropes. *Journal of Optometry*, 6(1), 36–44.
- 516 <https://doi.org/10.1016/j.optom.2012.07.001>
- 517 Elsner, A. E., Chui, T. Y. P., Feng, L., Song, H. X., Papay, J. A., & Burns, S. A. (2017).
- 518 Distribution differences of macular cones measured by AOSLO: Variation in slope from
- 519 fovea to periphery more pronounced than differences in total cones. *Vision Research*, 132,
- 520 62–68. <https://doi.org/10.1016/j.visres.2016.06.015>
- 521 Fiorentini, A., & Maffei, L. (1976). Spatial contrast sensitivity of myopic subjects. *Vision*
- 522 *Research*, 16(4), 437–438. [https://doi.org/10.1016/0042-6989\(76\)90214-5](https://doi.org/10.1016/0042-6989(76)90214-5)
- 523 Fujiwara, T., Imamura, Y., Margolis, R., Slakter, J. S., & Spaide, R. F. (2009). Enhanced Depth
- 524 Imaging Optical Coherence Tomography of the Choroid in Highly Myopic Eyes. *American*
- 525 *Journal of Ophthalmology*, 148(3), 445–450. <https://doi.org/10.1016/j.ajo.2009.04.029>
- 526 Gonzalez Blanco, F., Sanz Fernández, J. C., & Muñoz Sanz, M. A. (2008). Axial length, corneal
- 527 radius, and age of myopia onset. *Optometry and Vision Science*, 85(2), 89–96.
- 528 <https://doi.org/10.1097/OPX.0b013e3181622602>
- 529 Harb, E., Hyman, L., Gwiazda, J., Marsh-Tootle, W., Zhang, Q., Hou, W., ... Taylor, C. (2015).
- 530 Choroidal thickness profiles in myopic eyes of young adults in the correction of myopia
- 531 evaluation trial cohort. *American Journal of Ophthalmology*, 160(1), 62–71.e2.
- 532 <https://doi.org/10.1016/j.ajo.2015.04.018>
- 533 He, M., Zeng, J., Liu, Y., Xu, J., Pokharel, G. P., & Ellwein, L. B. (2004). Refractive error and
- 534 visual impairment in urban children in southern china. *Invest Ophthalmol Vis Sci*, 45(3),
- 535 793–799. <https://doi.org/10.1167/iovs.03-1051>
- 536 He, X., Zou, H., Lu, L., Zhao, R., Zhao, H., Li, Q., & Zhu, J. (2015). Axial length/corneal radius
- 537 ratio: Association with refractive state and role on myopia detection combined with visual
- 538 acuity in Chinese schoolchildren. *PLoS ONE*, 10(2), e0111766.
- 539 <https://doi.org/10.1371/journal.pone.0111766>
- 540 Iyamu, E., Iyamu, J., & Obiakor, C. I. (2011). The Role of Axial Length-Corneal Radius of
- 541 Curvature Ratio in Refractive State Categorization in a Nigerian Population. *ISRN*
- 542 *Ophthalmology*, 2011, 1–6. <https://doi.org/10.5402/2011/138941>
- 543 Jaworski, A., Gentle, A., Zele, A. J., Vingrys, A. J., & McBrien, N. A. (2006). Altered visual
- 544 sensitivity in axial high myopia: A local postreceptor phenomenon? *Investigative*
- 545 *Ophthalmology and Visual Science*, 47(8), 3695–3702. <https://doi.org/10.1167/iovs.05-1569>
- 546 Jong, M., Sankaridurg, P., Li, W., Resnikoff, S., Naidoo, K., & He, M. (2018). Reduced vision in

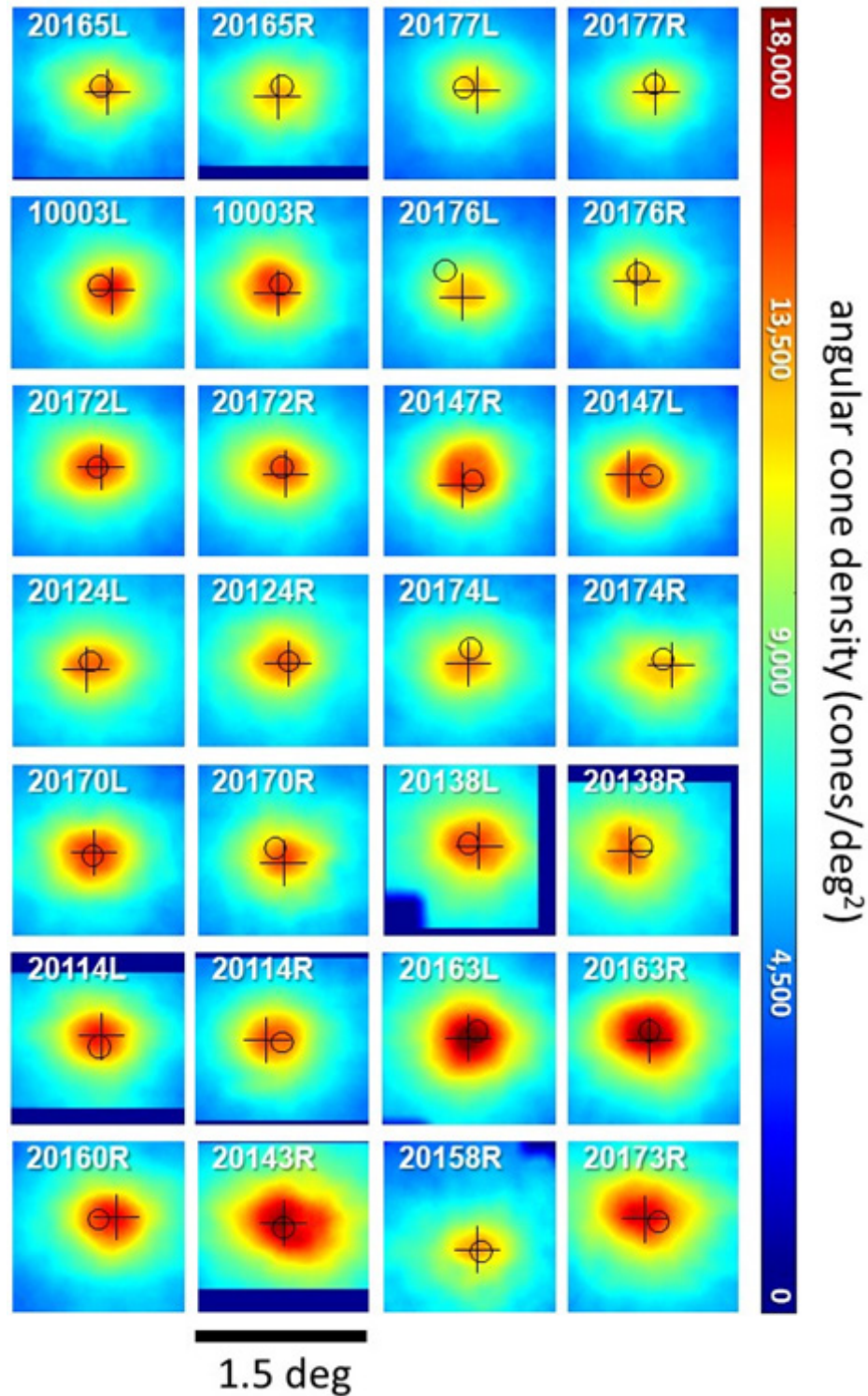
- 547 highly myopic eyes without ocular pathology: the ZOC-BHVI high myopia study. *Clin Exp*
548 *Optom*, 101(1), 77–83. <https://doi.org/10.1111/cxo.12563>
- 549 Kitaguchi, Y., Bessho, K., Yamaguchi, T., Nakazawa, N., Mihashi, T., & Fujikado, T. (2007). In
550 vivo measurements of cone photoreceptor spacing in myopic eyes from images obtained by
551 an adaptive optics fundus camera. *Japanese Journal of Ophthalmology*, 51(6), 456–461.
552 <https://doi.org/10.1007/s10384-007-0477-7>
- 553 Li, K. Y., & Roorda, A. (2007). Automated identification of cone photoreceptors in adaptive
554 optics retinal images. *Journal of the Optical Society of America A*, 24(5), 1358.
555 <https://doi.org/10.1364/JOSAA.24.001358>
- 556 Li, K. Y., Tiruveedhula, P., & Roorda, A. (2010). Intersubject variability of foveal cone
557 photoreceptor density in relation to eye length. *Investigative Ophthalmology and Visual*
558 *Science*, 51(12), 6858–6867. <https://doi.org/10.1167/iovs.10-5499>
- 559 Liang, J., Williams, D. R., & Miller, D. T. (1997). Supernormal vision and high-resolution
560 retinal imaging through adaptive optics. *Journal of the Optical Society of America A*,
561 14(11), 2884. <https://doi.org/10.1364/JOSAA.14.002884>
- 562 Liou, S.-W., & Chiu, C.-J. (2001). Myopia and contrast sensitivity function. *Current Eye*
563 *Research*, 22(2), 81–84. <https://doi.org/10.1076/ceyr.22.2.81.5530>
- 564 MacLeod, D. I. A., Williams, D. R., & Makous, W. (1992). A visual nonlinearity fed by single
565 cones. *Vision Research*, 32, 347–363. [https://doi.org/10.1016/0042-6989\(92\)90144-8](https://doi.org/10.1016/0042-6989(92)90144-8)
- 566 Meadway, A., & Sincich, L. C. (2018). Light propagation and capture in cone photoreceptors.
567 *Biomedical Optics Express*, 9(11), 5543. <https://doi.org/10.1364/boe.9.005543>
- 568 Morgan, I. G., Ohno-Matsui, K., & Saw, S. M. (2012). Myopia. *The Lancet*, 379(9827), 1739–
569 1748. [https://doi.org/10.1016/S0140-6736\(12\)60272-4](https://doi.org/10.1016/S0140-6736(12)60272-4)
- 570 Obata, R., & Yanagi, Y. (2014). Quantitative analysis of cone photoreceptor distribution and its
571 relationship with axial length, age, and early age-related macular degeneration. *PLoS ONE*,
572 9(3), e91873. <https://doi.org/10.1371/journal.pone.0091873>
- 573 Pallikaris, A., Williams, D. R., & Hofer, H. (2003). The reflectance of single cones in the living
574 human eye. *Investigative Ophthalmology and Visual Science*, 44(10), 4580–4592.
575 <https://doi.org/10.1167/iovs.03-0094>
- 576 Park, S. P., Chung, J. K., Greenstein, V., Tsang, S. H., & Chang, S. (2013). A study of factors
577 affecting the human cone photoreceptor density measured by adaptive optics scanning laser
578 ophthalmoscope. *Experimental Eye Research*, 108, 1–9.
579 <https://doi.org/10.1016/j.exer.2012.12.011>
- 580 Poletti, M., Listorti, C., & Rucci, M. (2013). Microscopic eye movements compensate for
581 nonhomogeneous vision within the fovea. *Current Biology*, 23(17), 1691–1695.
582 <https://doi.org/10.1016/j.cub.2013.07.007>
- 583 Poonja, S., Patel, S., Henry, L., & Roorda, A. (2005). Dynamic visual stimulus presentation in an
584 adaptive optics scanning laser ophthalmoscope. *Journal of Refractive Surgery*, 21(5), S575–
585 S580. <https://doi.org/10.1364/fio.2004.fthv3>
- 586 Putnam, N. M., Hammer, D. X., Zhang, Y., Merino, D., & Roorda, A. (2010). Modeling the
587 foveal cone mosaic imaged with adaptive optics scanning laser ophthalmoscopy. *Optics*
588 *Express*, 18(24), 24902–24916. <https://doi.org/10.1364/OE.18.024902>
- 589 Putnam, N. M., Hofer, H., Doble, N., Chen, L., Carroll, J., & Williams, D. R. (2005). The locus
590 of fixation and the foveal cone mosaic. *Journal of Vision*, 5(7), 632–639.
591 <https://doi.org/10.1167/5.7.3>
- 592 Roorda, A., Romero-Borja, F., Donnelly III, W. J., Queener, H., Hebert, T. J., & Campbell, M.

- 593 C. W. (2002). Adaptive optics scanning laser ophthalmoscopy. *Optics Express*, 10(9), 405.
594 <https://doi.org/10.1364/OE.10.000405>
- 595 Rossi, E. A., & Roorda, A. (2010a). Is visual resolution after adaptive optics correction
596 susceptible to perceptual learning? *Journal of Vision*, 10(12), 11.
597 <https://doi.org/10.1167/10.12.11>
- 598 Rossi, E. A., & Roorda, A. (2010b). The relationship between visual resolution and cone spacing
599 in the human fovea. *Nature Neuroscience*, 13(2), 156–157. <https://doi.org/10.1038/nn.2465>
- 600 Rossi, E. A., Weiser, P., Tarrant, J., & Roorda, A. (2007). Visual performance in emmetropia
601 and low myopia after correction of high-order aberrations. *Journal of Vision*, 7(8), 14.
602 <https://doi.org/10.1167/7.8.14>
- 603 Scoles, D., Sulai, Y. N., Langlo, C. S., Fishman, G. A., Curcio, C. A., Carroll, J., & Dubra, A.
604 (2014). In vivo imaging of human cone photoreceptor inner segments. *Investigative*
605 *Ophthalmology and Visual Science*, 55(7), 4244–4251. [https://doi.org/10.1167/iovs.14-](https://doi.org/10.1167/iovs.14-14542)
606 [14542](https://doi.org/10.1167/iovs.14-14542)
- 607 Springer, A. D., & Hendrickson, A. E. (2004). Development of the primate area of high acuity. 1.
608 Use of finite element analysis models to identify mechanical variables affecting pit
609 formation. *Visual Neuroscience*, 21(1), 53–62. <https://doi.org/10.1017/S0952523804041057>
- 610 Stevenson, S. B., & Roorda, A. (2005). Correcting for miniature eye movements in high
611 resolution scanning laser ophthalmoscopy. *Ophthalmic Technologies XV*, 5688, 145.
612 <https://doi.org/10.1117/12.591190>
- 613 Stoimenova, B. D. (2007). The Effect of Myopia on Contrast Thresholds. *Investigative*
614 *Ophthalmology & Visual Science*, 48(5), 2371. <https://doi.org/10.1167/iovs.05-1377>
- 615 Strang, N. C., Winn, B., & Bradley, A. (1998). The role of neural and optical factors in limiting
616 visual resolution in myopia. *Vision Research*, 38(11), 1713–1721.
617 [https://doi.org/10.1016/S0042-6989\(97\)00303-9](https://doi.org/10.1016/S0042-6989(97)00303-9)
- 618 Thorn, F., Corwin, T. R., & Comerford, J. P. (1986). High myopia does not affect contrast
619 sensitivity. *Curr Eye Res*, 5(9), 635–639. Retrieved from
620 <http://www.ncbi.nlm.nih.gov/pubmed/3769528>
- 621 Troilo, D. (1998). Changes in retinal morphology following experimentally induced myopia.
622 *Vision Science and Its Applications: Technical Digest (OSA, Washington, D.C.)*, 1(1), 206–
623 209.
- 624 Verkicharla, P. K., Ohno-Matsui, K., & Saw, S. M. (2015). Current and predicted demographics
625 of high myopia and an update of its associated pathological changes. *Ophthalmic and*
626 *Physiological Optics*. <https://doi.org/10.1111/opo.12238>
- 627 Vitale, S. (2009). Increased Prevalence of Myopia in the United States Between 1971-1972 and
628 1999-2004. *Archives of Ophthalmology*, 127(12), 1632.
629 <https://doi.org/10.1001/archophthamol.2009.303>
- 630 Vojnikovic, B., & Tamajo, E. (2013). Gullstrand's optical schematic system of the eye--modified
631 by Vojnikovic & Tamajo. *Coll Antropol*, 37 Suppl 1, 41–45. Retrieved from
632 <http://www.ncbi.nlm.nih.gov/pubmed/23841130>
- 633 Webb, R. H., Hughes, G. W., & Delori, F. C. (1987). Confocal scanning laser ophthalmoscope.
634 *Applied Optics*, 26(8), 1492. <https://doi.org/10.1364/AO.26.001492>
- 635 Wilk, M. A., Dubis, A. M., Cooper, R. F., Summerfelt, P., Dubra, A., & Carroll, J. (2017).
636 Assessing the spatial relationship between fixation and foveal specializations. *Vision*
637 *Research*, 132, 53–61. <https://doi.org/10.1016/j.visres.2016.05.001>
- 638 Williams, D. R. (1985). Aliasing in human foveal vision. *Vision Research*, 25, 195–205.

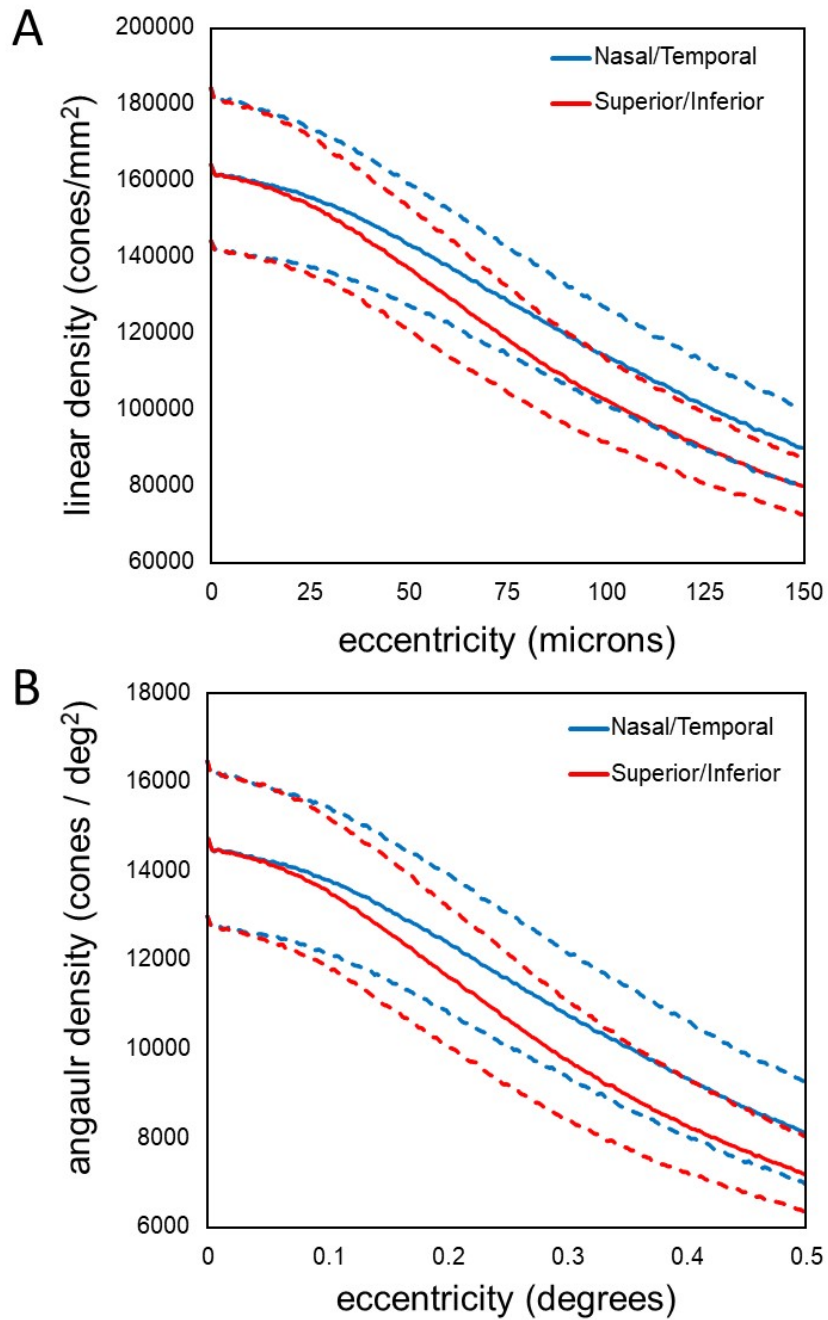
639 [https://doi.org/10.1016/0042-6989\(85\)90113-0](https://doi.org/10.1016/0042-6989(85)90113-0)
640 Zhang, T., Godara, P., Blanco, E. R., Griffin, R. L., Wang, X., Curcio, C. A., & Zhang, Y.
641 (2015). Variability in Human Cone Topography Assessed by Adaptive Optics Scanning
642 Laser Ophthalmoscopy. *American Journal of Ophthalmology*.
643 <https://doi.org/10.1016/j.ajo.2015.04.034>
644
645



646
647 **Supplemental Figure 1:** Linear cone density (cones/mm²) plots over the central 450 microns for
648 all 28 subjects. The black cross indicates the point of maximum cone density. The black circle
649 indicates the PRL location. Dark blue regions indicate where no cone density estimates were
650 made.
651



652
653 **Supplemental Figure 2:** Angular cone density (cones/deg²) plots over the central 1.5 degrees for
654 all 28 subjects. The black cross indicates the point of maximum cone density. The black circle
655 indicates the PRL location. Dark blue regions indicate where no cone density estimates were
656 made.
657



658
659 **Supplemental Figure 3:** Plots of density as a function of eccentricity in the vertical and
660 horizontal directions. (A) linear cone density (B) angular cone density. The dashed lines
661 represent +/- 1 standard deviation from the mean.